Materials Advances

ROYAL SOCIETY OF CHEMISTRY

PAPER

View Article Online
View Journal | View Issue



Cite this: *Mater. Adv.*, 2025, 6, 2170

# Magnetic activated carbon particles as stimuli-responsive vehicles for methotrexate†

J. A. Lirio Piñar, ‡[ab] M. Lázaro,‡[abc] G. R. Iglesias, [abcd] Tania Romacho,[e] A. V. Delgado, [abcd] Gracia García-García*[be] and S. Ahualli *[ad]

Received 15th October 2024,
Accepted 22nd February 2025

DOI: 10.1039/d4ma01037j

rsc.li/materials-advances

This study investigates porous activated carbon (AC) particles as drug delivery vehicles for methotrexate (MTX). To enhance functionality, magnetic nanoparticles are embedded in AC imparting superparamagnetic properties (MAC composites), making them suitable for controlled transport and localization, as well as for facilitating their response to external fields. The composites are further functionalized with branched low molecular weight polyethyleneimine (PEI) to confer them a positive charge. After characterizing size, composition, and magnetic hysteresis, their potential as MTX carriers is assessed. Electrophoretic mobility and infrared data confirm the presence of magnetite, polymer, and drug molecules. Photothermal therapy (PTT) tests reveal that MAC–PEI particles produce up to 180 W $g^{-1}$ of specific absorption rate (SAR) under infrared laser radiation. Due to its anisotropy, rotating magnetic fields (RMF) induce particle rotation, offering another external stimulus. Biocompatibility studies with human skin M1 fibroblasts confirm no significant cytotoxicity at concentrations below 700 μg $mL^{-1}$. The particles adsorb over 80% of MTX from 0.6 mM solutions, with release evaluated at pH 5.8 under PTT and RMF stimuli. Both methods significantly enhance MTX release, achieving twice the drug release compared to passive conditions, demonstrating the particles' high potential as active vehicles for targeted MTX delivery.



## 1. Introduction

Cancer is one of the world's leading causes of death and its incidence is expected to triple by 2050, largely due to ageing population.[1,2] It is therefore evident that novel approaches are required to overcome the forthcoming challenges in cancer treatment. A promising strategy to address this issue involves the use of advanced carriers with the objective of optimizing conventional treatments (*e.g.* chemotherapy) and/or the implementation of novel therapeutic approaches such as antitumor hyperthermia.[3–9]

Methotrexate (MTX) is a standard anticancer drug employed in the treatment of a range of cancers, including acute lymphoblastic leukemia,[10] osteosarcoma,[11] and lymphoma malignancies,[12] among others. However, MTX is subject to rapid plasma clearance and poor solubility,[13] necessitating the administration of high doses over an extended infusion period to achieve effective treatment. Consequently, this dosage regimen is frequently associated with toxic effects and the development of resistance.[14–16] Therefore, the controlled delivery of MTX is being investigated as a means of enhancing the safety and efficacy of therapy.[17]

Among the potential advanced materials for MTX delivery, carbon-based microporous (pore size in the order of a few nm) particles have shown promise.[18–20] The nanometer pore diameter of AC materials is responsible for a high surface area to volume ratio, which renders them potential candidates for high drug payloads, as has been previously reported.[21,22] In addition, AC particles possess a larger diameter pore structure, known as mesopores (2–50 nm) and macropores (above 50 nm), sufficiently large to accommodate large molecules, such as various drugs, including MTX.

Moreover, AC particles are cost-effective and safe, and they are already being employed in clinical settings.[23] In addition to their potential for drug delivery, they are capable of absorbing light within the NIR-I window, where tissues are nearly transparent, and converting it into heat. For example, Shahcheragh *et al.*[24] demonstrated a strong absorbance in the 300–1100 nm wavelength range. Furthermore, Li *et al.*[25] developed an innovative

[a] *Department of Applied Physics, School of Sciences, University of Granada, 18071 Granada, Spain. E-mail: sahualli@ugr.es*
[b] *NanoMag Lab. Department of Applied Physics, Faculty of Science University of Granada, Planta -1. Edificio I + D Josefina Castro, Av. de Madrid, 28, 18012 Granada, Spain*
[c] *Biosanitary Research Institute of Granada (ibs.GRANADA), Andalusian Health Service (SAS), University of Granada, 18001 Granada, Spain*
[d] *MNat Unit of Excellence, University of Granada, Spain*
[e] *Chronic Complications Diabetes Lab (ChroCoDiL), Department of Nursing, Physiotherapy and Medicine, University of Almería, Ctra. Sacramento s/n, 04120 Almería, Spain. E-mail: graciagg@ual.es*

† Electronic supplementary information (ESI) available. See DOI: https://doi.org/10.1039/d4ma01037j

‡ These authors contributed equally to this work.

approach whereby the incorporation of carbon nanoparticles (NPs) facilitated the enhanced absorption of laser irradiation on a suspension of (low-absorbance) alumina, resulting in the production of particles with precisely controlled geometry.

In this work, interest is focused on achieving a local temperature elevation by application of external stimuli capable of releasing heat. This is a controlled way of reaching hyperthermia (temperature above 37.5 °C), and it is denominated photothermal therapy (PTT) when it is achieved by subjecting the target system to the action of a laser radiation, typically in the near-infrared (NIR) range. While other potential applications exist, most research efforts in the field of PTT are concentrated on the biomedical domain. The objective is to achieve localized heating, which can effectively eliminate malignant cells without affecting surrounding healthy tissue. This can be achieved through direct application of an infrared laser to skin tumors or indirectly to deeper tumors using techniques such as optical fibers, which can guide the light directly into the malignant area. While PTT has been the subject of extensive preclinical investigation (see, for example, ref. 26 and 27), ongoing research is aimed at facilitating its translation into clinical applications.[28]

Iron oxide NPs (magnetite and maghemite) have been the subject of extensive investigation due to their superparamagnetic and biocompatible character, with applications in drug delivery, magnetic resonance imaging (MRI), and magnetic hyperthermia.[29] It is noteworthy that magnetite NPs also demonstrate a photothermal therapy response, as evidenced in previous studies.[30–33] Furthermore, it has recently been reported that a low-frequency magnetic field applied to drug-loaded magnetic particles has the potential to induce a prompt release of the drug. In such circumstances, the magnetic particles align themselves with the direction of the rotating field, thereby generating a strong mechanical force that is capable of producing a rapid release of the drug.[34,35] In addition, *in vitro*[36] and *in vivo*[37] antitumor effect of magnetic particles under a low-frequency magnetic field have been recently demonstrated.

Polyethyleneimine (PEI) has been shown to be an effective coating agent for inorganic nanoparticles in a number of studies.[33,38–41] It is a versatile, highly positive charge-density polycation that creates a cationic surface, which has particular interest in the field of anticancer drug delivery. A positive surface can facilitate enhanced biological interactions with cellular surfaces, thereby improving cellular uptake. Additionally, it can facilitate interactions with tumor vasculature proteoglycans, which could improve specific targeting.[42] Furthermore, the characteristics of this polymer are highly advantageous for drug delivery, particularly due to its hydrophilic nature and its capacity to load negatively charged drugs such as MTX, as previously reported.[43] Furthermore, and of greater relevance to the intended application, it endows the system with biocompatibility, given that low-molecular-weight branched PEI exhibits low cytotoxicity.[44,45]

This article proposes a method for the production of activated carbon (AC) microporous particles that are magnetizable (magnetic activated carbons, or MAC) through the incorporation of magnetic iron oxide NPs. It has been previously demonstrated that carbon materials in the form of carbon nanodots, with different doping elements and surface modifications, are efficient carriers for drugs like camptothecin,[46–48] with significant *in vitro* anticancer activity.

The physicochemical and magnetic characterization of the particles confirm their structure, demonstrating an appropriate size, composition, and PTT and magnetic character. The PEI surface coating of MAC was employed to enhance the particles' interaction with MTX, given that this exhibits a negative charge. Moreover, the MAC–PEI structures demonstrated preliminary biocompatibility, as evidenced by the absence of cytotoxic effects in the human skin fibroblast cell line M1 in a broad concentration range (0–700 μg $mL^{-1}$). Finally, *in vitro* drug release studies demonstrated the potential of MTX-loaded MAC–PEI for stimuli-responsive drug delivery when an external NIR-I light or a low-frequency rotating magnetic field was applied. To the best of our knowledge, this is the first instance of a hybrid nanomaterial based on AC, magnetic nanoparticles and PEI having been engineered. To date, no studies have focused on the MTX adsorption and release of this material and the effect of PTT and low-strength rotating magnetic field stimuli. It is the objective of this research to facilitate the clinical translation of MAC particles as anticancer agents under external stimuli.

## 2. Materials and methods

### 2.1. Materials

YP50F AC particles were purchased from Kuraray Europe GmbH (Finland). The iron salts $FeSO_4{\cdot}7H_2O$ and $FeCl_3{\cdot}6H_2O$ from Merck Sigma Aldrich (Germany), and a 32% ammonia solution from Scharlau, Spain were used for the preparation of the magnetic NPs, together with water from a Milli-Q academic device (Millipore, Spain). For the polymer coating, branched polyethyleneimine (PEI, MW ≈ 2000 g $mol^{-1}$) was used, and for the drug adsorption and release experiments methotrexate (MTX) was chosen, both compounds from Sigma Aldrich (Germany). Phosphate buffer saline (PBS), glutaraldehyde, acetic acid, crystal violet solution (1%, aqueous solution) and antibiotic–antimycotic solution (10 000 units penicillin, 10 mg streptomycin and 25 μg amphotericin B per mL) for cell culture and biocompatibility tests were also from Merck Sigma-Aldrich (Ger), and Dulbecco's modified Eagle's medium (DMEM), fetal bovine serum (FBS), 0.05% trypsin-EDTA were supplied by GibcoTM (ThermoFisher Scientific, USA).

### 2.2. Methods

**2.2.1. Preparation of polyethyleneimine-coated magnetic activated carbon particles preparation.** The synthesis of $Fe_3O_4$ colloids was conducted in accordance with the chemical co-precipitation methodology previously reported in ref. 46. Magnetic activated carbon (MAC) particles were produced by the addition of YP50F AC to the aqueous media in which the $Fe_3O_4$ colloids were formed. The methodology commenced with the mechanical stirring of two aqueous solutions, comprising 0.9 g of $FeSO_4{\cdot}7H_2O$ in 8.6 mL and 1.7 g of $FeCl_3{\cdot}6H_2O$ in 10 mL, respectively,

at room temperature. Subsequently, 5.2 g of YP50F AC was dispersed in 100 mL of water and added to the aforementioned solutions. The resulting suspension was then stirred for a period of 30 minutes. To induce the precipitation of $Fe_3O_4$ onto the surface of the AC particles, 4.4 mL of the ammonia solution was added. Following a period of one hour under mechanical stirring, the resulting MAC particles were subjected to three cycles of centrifugation (10 minutes at 15 000 rpm, using a Sigma 3-30KS centrifuge, Germany), followed by magnetic decanting and redispersion in water. Subsequently, the product was subjected to drying in an oven at a temperature of 50 degrees celsius.

In order to obtain the MAC particles coated with the PEI polymer, 0.5 g of MAC particles were diluted in 30 mL of PEI, and MilliQ water was added to complete a solution of 250 mL. The mixture was then subjected to rigorous mechanical stirring for the duration of the night. Subsequently, the particles were purified by centrifugation at 21 000 rpm for 20 minutes, with this process repeated until the supernatant reached a pH range of 7–7.5.

**2.2.2. Adsorption of methotrexate onto the surface of polyethyleneimine-coated magnetic activated carbon particles.** MTX-loaded MAC–PEI nanoporous particles were produced by the incubation of MAC particles (6 mg $mL^{-1}$) in an aqueous solution containing MTX (0.6 mM) under mild stirring using a stuart rotator SB3 (United States) at 30 rpm (Fig. 1). Samples were centrifuged for 45 minutes at 14 000 rpm (Mikro 220R, Hettich Zentrifugen, Germany) to remove the non-attached drug molecules. Two adsorption kinetics experiments were performed, the first one at a fixed concentration (the one chosen for the rest of the experiments, 0.6 mM MTX) *versus* time, in the range of 1, 2, 24, 72, 144 hours. The second one, at a fixed time (24 hours of adsorption) varying the drug concentration (between 0.2 mM–10 mM). Fig. 1a provides a schematic representation of the process of MAC particle synthesis, coating with PEI, and drug incorporation.

**2.2.3. Size and shape of the particles.** Evaluation of the size of the MAC nanoplatforms was carried out by electron microscopy analysis. $Fe_3O_4$ and MAC particles were studied by high-resolution transmission electron microscopy (HRTEM) and high-angle annular dark field scanning transmission electron microscopy (HAADF-STEM) (HAADF TALOS F200X, Thermofisher Scientific Inc., United States; accelerating voltage of 200 kV). Elemental analysis was performed during these electron microscopy observations [energy dispersive X-ray (EDX) spectrometer, Bruker Nano GmbH, Germany]. Particle size was also evaluated by dynamic light scattering (DLS) using a Zetasizer Nano-ZS (Malvern Pananalytical, UK). The specific surface area of AC YP50F is 1692 $m^2\ g^{-1}$, and the micropore size distribution peaks at 1 nm (according to Kuraray Europe GmbH). These characteristics make it an ideal drug vehicle.[49]

**2.2.4. Electrophoretic mobility.** The determination of the surface electrical properties of AC, bare $Fe_3O_4$, MAC–PEI and MTX-loaded MAC–PEI was carried out by measuring their electrophoretic mobility using the Zetasizer Nano-ZS device. A qualitative follow-up of the PEI coating of the MAC surface and the subsequent MTX adsorption was carried out by determining the influence of pH on their electrophoretic mobility in the presence of 1 mM KCl.

**2.2.5. FTIR analysis.** The structure of MAC–PEI was confirmed by Fourier transform infrared (FTIR) spectroscopy (FT/IR-6200 spectrometer, JASCO, United States; resolution of 0.25 $cm^{-1}$). For that purpose, the MAC–PEI spectrum was compared to those obtained for MAC, $Fe_3O_4$ and PEI.

**2.2.6. Magnetic properties.** The magnetization cycles were obtained at (20.0 ± 0.5) °C, in both a vibrating sample magnetometer (PPMS DynaCool, Quantum Design, USA, maximum applied field strength 4700 kA $m^{-1}$) and an AC Hyster Series magnetometer (Nanotech Solutions S.L., Spain), operating at a frequency of 1.5 kHz and a maximum field strength of 120 kA $m^{-1}$.

**2.2.7. Low-frequency rotating magnetic field application.** The technique entails exposing the sample to a low-frequency RMF, thereby circumventing the heating phenomenon that occurs in magnetic hyperthermia. This approach facilitates

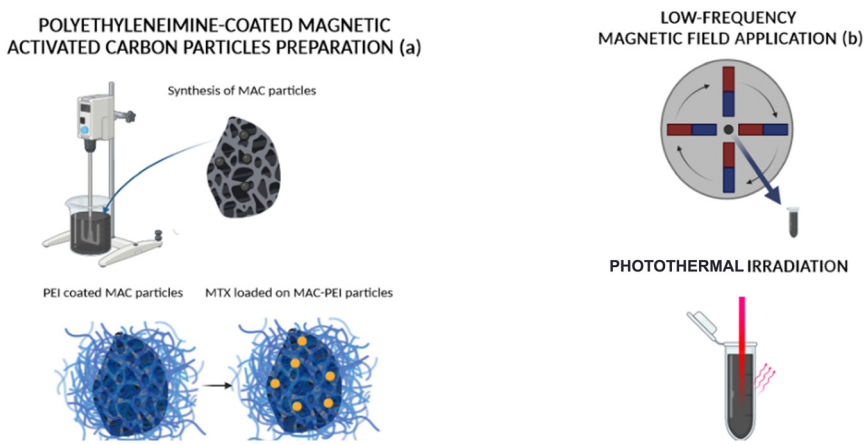


Fig. 1 (a) Scheme of the synthesis procedures of MAC particles, their coating with PEI, and the incorporation of pharmacophore. (b) Diagram of the operation of the low-frequency rotating magnetic field device (top) and of the photothermia experiment (below). Images created with **https://Biorender.com**.

drug release by rotating the particles, which enhances the diffusion process. This is accomplished through the utilisation of four permanent magnets positioned in a face-to-face configuration. The magnets are made to rotate in synchrony around the sample, with opposite polarities (Fig. 1b). The synchronised rotation of the magnetic field induces a corresponding rotation of the magnetic particles within the sample. The field strength was 65 mT and the rotation speed 300 ± 10 rpm.

**2.2.8. Thermal measurements.** The photothermal (PTT) capacity of the various samples was evaluated using an 850 nm laser at powers of 0.5, 1 and 1.5 W $cm^{-2}$. The particle concentrations were 5 mg $mL^{-1}$. Eppendorf tubes containing 100 μl of the nanoparticles ($Fe_3O_4$, AC, MAC and MAC–PEI particles) in water were used. Irradiation was conducted from the top, and the temperature was recorded with a thermographic camera (FLIR E60, 320 × 240 pixel IR resolution, FLIR Systems, Inc., United States) throughout the experiment (Fig. 1).

The amount of heat transferred from the particles to their surrounding environment is determined by the specific absorption rate (SAR), which is calculated through experimental means as follows:

$$\mathrm{SAR} = \frac{C_{\mathrm{liq}}\rho_{\mathrm{liq}}}{\varphi}\frac{\mathrm{d}T}{\mathrm{d}t} \quad (1)$$

being $C_{\mathrm{liq}}$,$\rho_{\mathrm{liq}}$ the mass specific heat and the density of the suspension and $\phi$ the NPs concentration (w/v). The essential quantity is the rate of temperature increase $\mathrm{d}T/\mathrm{d}t$, which is determined by the linear model.[50] The densities of magnetite ($\rho_{\mathrm{MAG}}$ = 5.2 × $10^3$ g $L^{-1}$), and of AC ($\rho_{\mathrm{AC}}$ = 0.3 × $10^3$ g $L^{-1}$, provided by Kuraray Europe GmbH), as well as the magnetite-to-carbon ratio for the MAC sample were used for the SAR determination.

**2.2.9. Magnetic activated carbon platforms as methotrexate delivery systems.** In order to determine the concentration of MTX after adsorption, a calibration set of absorbance *versus* concentration data was obtained by measuring the optical absorbance at 305 nm (maximum absorbance wavelength for MTX) using a BioSpectrometer kinetic UV/VIS spectrophotometer (Eppendorf AG, Germany) for the concentrations used in the range of 0.001–0.2 mM of MTX.

Drug release experiments were conducted using MTX-loaded MAC–PEI particles (1.5 mL suspensions containing 6 mg $mL^{-1}$ of particles) under two different conditions: physiological (pH 7.4 phosphate buffer) and tumour-like (pH 5.8 phosphate buffer). To this end, 1.3 mL of the medium was withdrawn at predetermined intervals for UV spectrophotometric analysis. An equal volume of the release medium, maintained under the same conditions, was added after sampling to maintain the final volume (sink conditions[41]), and the release process was continued. When necessary, the laser for photothermia and/or the RMF were applied while the release process was taking place.

**2.2.10. Cell culture and cytotoxicity assay.** Cells from the human fibroblast-derived, non-tumor epithelial cells and not commercial M1 cell line were cultured in DMEM pH 7.4, supplemented with 10% (v/v) FBS and antibiotic–antimycotic solution (0.2%) as previously described.[51] Cells were incubated at 37 °C with 5% $CO_2$. Medium was changed every 48 h, unless stated.

MAC–PEI particles potential cytotoxicity was determined by crystal violet, following a previously described protocol.[33] M1 cells were grown in a 96-well plate (25.000 cells per well) at 37 °C with 5% $CO_2$ during 24 h. Then, cells were exposed to a broad concentration range (0–1000 μg $ml^{-1}$) of previously UV-and ethanol sterilized MAC–PEI particles. After 24 h incubation, the medium was removed from each well by aspiration cells washed with sterile PBS and were fixed with glutaraldehyde (1%) for 15 min. Glutaraldehyde was then washed with PBS 4×. Excess of PBS was removed by plate decantation and crystal violet (0.1% v/v) was added, incubated for 20 min and repeatedly washed with deionized water until no colour was leaking from the plate. The plate was dried overnight, the remaining dye was solubilized with 10% acetic acid and loaded per triplicates in a new 96 well plate. Absorbance was measured in each well at 590 nm with a microplate reader spectrophotometer (INNO, LTek, Korea).

Statistical analysis was carried out using one-way ANOVA followed by Bonferroni test to determine statistical significance ($p \leq 0.05$). All statistical analysis were performed using GraphPad Prism (version 10.1.2, La Jolla, CA, USA).

# 3. Results and discussion

## 3.1. Characterization

**3.1.1. Particle geometry.** $Fe_3O_4$ and MAC particle sizes determined by HRTEM were found to be (6.59 ± 0.22) nm (Fig. 2a) and (230 ± 170) nm, respectively (Fig. 2b and c). These average sizes were determined by measuring at least 20 particles in different pictures using JImage software. EDX mapping of Fe and C employing HAADF-STEM imaging demonstrated that the magnetite (represented by Fe element) is distributed over specific areas of the carbon surface (represented by C element) in the MAC particles (Fig. 2d–f). The sizes obtained by DLS were also measured (Fig. S1, ESI†), obtaining (74 ± 28) nm for magnetite, (355 ± 74) nm for carbon, (390 ± 170) nm for MAC and (590 ± 120) nm for MAC–PEI.[52]

**3.1.2. Electrical surface characteristics.** Electrophoretic mobility measurements of bare magnetite $Fe_3O_4$, AC, MAC and MTX-loaded MAC in 1 mM KCl served as qualitative assessment of the surface changes during the preparation procedure steps (Fig. 3). In accordance with previous studies, negative and neutral electrophoretic mobility was found for AC and bare $Fe_3O_4$, respectively.[53] When AC particles were decorated with $Fe_3O_4$ colloids following the coprecipitation method, the zeta potential values of the particles shifted from highly negative to moderate values, closer to those obtained for bare $Fe_3O_4$. This could be explained by the coverage of $Fe_3O_4$ onto AC surface, as demonstrated by EDX mapping analysis (Fig. 2f). As expected, the PEI coating causes the mobility to move towards slightly more positive values, this being in fact a qualitative proof of the achieved coating.[41] Finally, MTX-loaded MAC particles depicted more moderately negative values than non-loaded ones.[54]

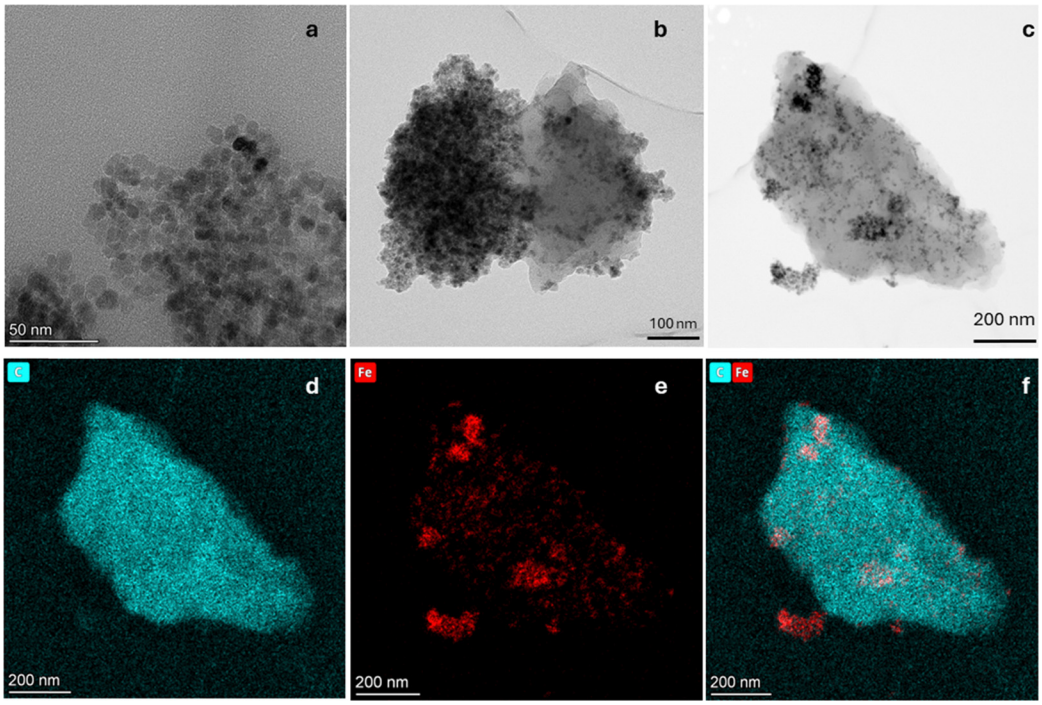


Fig. 2 HRTEM pictures of bare $Fe_3O_4$ and MAC platforms. (a) bare $Fe_3O_4$; (b) and (c) MAC; (d) EDX mapping analysis of C element of MAC particles; (e) EDX mapping analysis of Fe element of MAC particles; (f) EDX mapping analysis of overlapped C and Fe elements of magnetic carbon activated nanoplatforms.

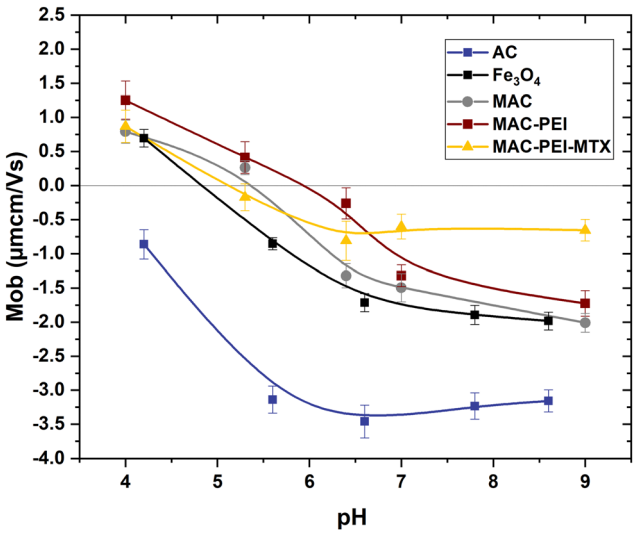


Fig. 3 Electrophoretic mobility measurements of bare $Fe_3O_4$, AC, MAC and MTX-loaded MAC (1 mM KCl).

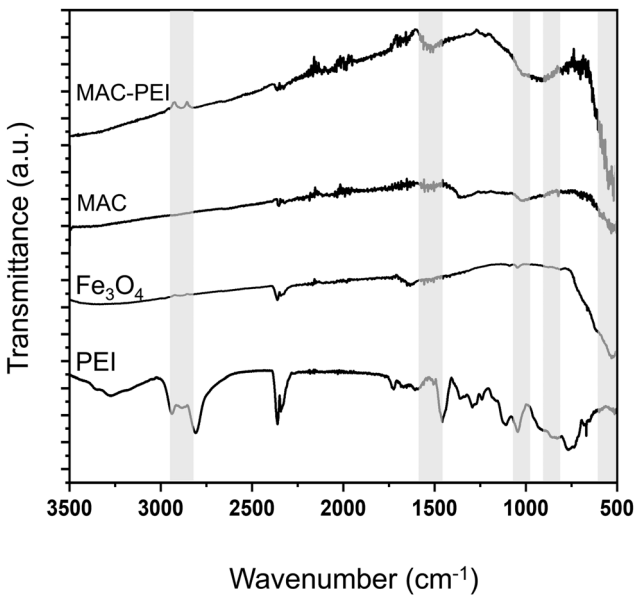


Fig. 4 FTIR analysis of the particles investigated.

Potential conjugation between MAC and MTX through interaction of the MAC –COOH groups and MTX $–NH_2$ groups could explain that behavior, as it has been previously reported.[20]

**3.1.3. Infrared analysis.** The MAC–PEI nanoporous particles were characterized by FTIR (Fig. 4). The IR transmittance spectra matched well with the data already reported in the literature.[55–58] The following analysis focuses on the most significant peaks that enable the identification of each material used. Symmetric and asymmetric C–H stretching vibrations of the fatty $CH_2$ on the PEI backbone signal were identified in the IR spectrum of MAC–PEI and PEI, at 2970 and 2894 $cm^{-1}$. Then, at 1635 $cm^{-1}$, the stretching vibration of C═O in the carboxyl group appeared for MAC and MAC–PEI. AC presence in MAC and MAC–PEI was also confirmed by the absorption peak located at 1020 $cm^{-1}$, as it is characteristic of some

oxygen-containing functional groups. Because of that, this peak can also be observed in the $Fe_3O_4$ spectrum. PEI coating was again identified at 881 $cm^{-1}$, as an absorption peak appeared corresponding to the stretching vibration of the N–H bond in the PEI amine group. Finally, the absorption bands of the region around $\approx$550 $cm^{-1}$ are attributed to the stretching vibrations of metal oxide (Fe–O) bonds.

### 3.2. Magnetic characterization

Magnetic characterization results of bare $Fe_3O_4$, MAC and PEI coated particles are depicted in Fig. 5a. It can be observed that the magnetization of magnetite nanoparticles is 65 emu $g^{-1}$, somewhat lower than that of bulk magnetite and the value reported by other authors,[59] probably due to a slight oxidation to maghemite, since the synthesis process is carried out in the presence of oxygen. The results obtained by the two methods are coherent, except for the range of magnetic field applied. In all cases, the increasing and decreasing field ramps are almost coincident, suggesting a superparamagnetic character of the magnetite NPs, a feature that is transferred to the magnetic carbon hybrid particles, as depicted in the low field detail of Fig. 5b. The low magnetic hysteresis of the composites suggests a potential application of the MAC particles for biomedical purposes, given their moderate magnetization and their expectedly negligible risk of aggregation in blood vessels due to magnetic forces.[29] This is also an indication of an efficient coating of the AC particles by magnetite, although the saturation magnetization of the former (6.0 $\pm$ 0.2 emu $g^{-1}$) is considerably lower due to the comparatively small mass of magnetic material.

In addition, the AC maximum magnetization of PEI-coated MAC particles was also determined, obtaining a very similar value (7.9 $\pm$ 0.3 emu $g^{-1}$), although slightly higher, probably due to the increased stability of the suspension (MAC particles tended to sediment quickly) (Fig. 5a and b). This is because PEI is a sterically branched polymer with numerous amino groups, which are hydrophilic and capable of forming hydrogen bonds with water.[60–62] This characteristic provides stability to the NPs in the dispersion medium, due to the strong electrostatic repulsion forces between them, thus preventing their aggregation. Note in Fig. S1 (ESI†) the narrower size distribution of MAC–PEI composites, as compared to bare activated carbon particles. The slightly increased average size of MAC–PEI suggests that the PEI layer is thin enough to provide stability and biocompatibility without significantly increasing the particle dimensions.

### 3.3. Photothermal response

Experimental conditions were carefully selected regarding clinical safety limits for photothermia. A wavelength in the first biological transparency window (NIR-I) was chosen, in addition to laser power densities within the range of acceptable values previously reported.[26,63–65] Therefore, our research was focused on evaluating the impact of heating induced by NPs at mild conditions where the impact of tissue damage caused solely by the laser power irradiation would be negligible.

As can be seen in Fig. 6a–c, magnetic NPs are an excellent heating agent in photothermal therapy, as has been demonstrated previously by several authors.[26,66,67] Moreover, their magnetic properties allow them to be directed with an external field. In the case of activated carbon alone, the temperature rise and hence the SAR achieved is certainly lower, although considering its advantageous high surface area, AC particles cannot be neglected as tools in photothermia.[68] What is particularly interesting is the PTT behavior of MAC particles. These retain the photothermal response of magnetite and, thanks to their content of AC, also have a high specific surface area. It is worth mentioning that for bare $Fe_3O_4$, MAC and MAC–PEI samples, the results obtained are always very similar, MAC–PEI always presenting a slightly better performance. This demonstrates the advantage of the polymer coating, since the layer is thin enough not to affect the amount of magnetite or carbon present in the sample, but provides greater stability, resulting in better PTT results, as was also observed in the electrophoretic mobility (Section 3.1.2), and in the magnetic characterization (Section 3.2).

On the other hand, the SAR determination (Fig. 6d), becomes another evidence of how the incorporation of

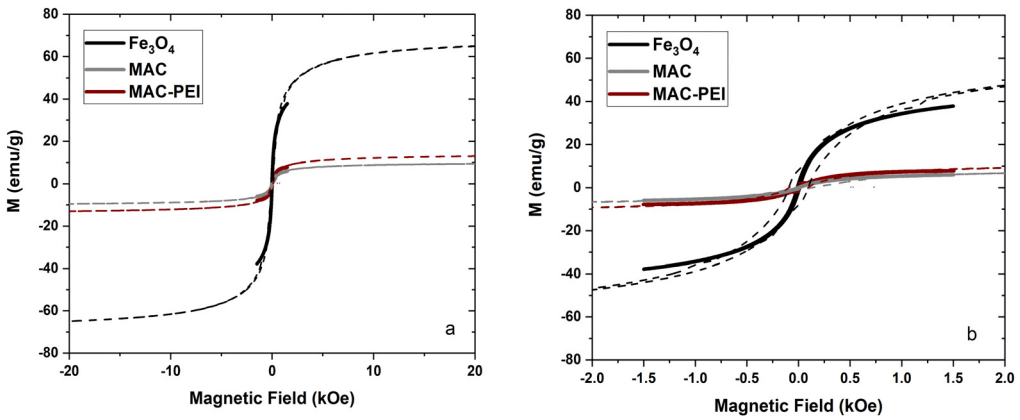


Fig. 5 Magnetic characterization of the obtained MAC nanoporous particles. (a) Magnetization curves of the bare $Fe_3O_4$, MAC and PEI coated particles using VSM (dotted lines) and AC magnetometry (solid lines); (b) low-field detail of the plots in (a). Hysteresis cycles carried out at 300 K.

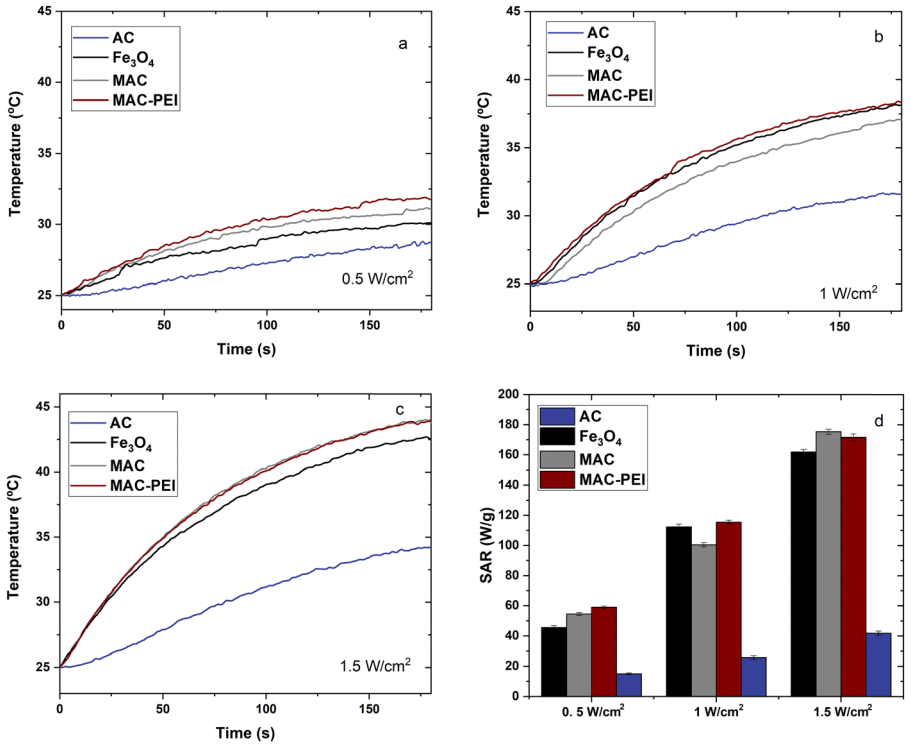


Fig. 6 Temperature increases for PTT therapy, at a power irradiation of 0.5 W $cm^{-2}$ (a), 1 W $cm^{-2}$ (b), and 1.5 W $cm^{-2}$ (c), using 100 μL of sample at 5 mg $mL^{-1}$. Determination of the SAR obtained (d).

magnetite is necessary to improve the photothermal response of activated carbon, as in most cases a higher SAR is obtained for magnetite/carbon composite particles than for magnetite alone. It should be mentioned that for the determination of the SAR of MAC and MAC–PEI samples it has been considered that approximately 86% of the sample is activated carbon, while 14% is magnetic material (as estimated from the saturation magnetizations in Fig. 5a).

In addition to the characterization performed, it is important to consider that drug release experiments are carried out with a much larger sample volume, which can affect the heating produced. Therefore, a comparative test was performed using 1.5 mL of sample (Fig. S2, ESI†), in which it was observed that the temperature increase obtained is again sufficient to reach the hyperthermia region (between 42 and 46 °C) (Fig. S2, ESI†).

### 3.4. Cell viability of the magnetic activated carbon nanoporous particles

Cell viability experiments were performed to determine whether the MAC–PEI nanoporous particles obtained provided the necessary biocompatibility. For this purpose, human skin M1 fibroblasts were plated. After 24 h, cells were exposed to different concentrations (from 25 to 1000 μg $mL^{-1}$) of MAC–PEI particles. This evaluation of the potential cytotoxic effects of MAC–PEI was based on the quantification of viable cells by crystal violet. Viable cells are stained with the dye, in contrast to non-viable ones. Increasing concentrations of MAC–PEI nanoporous particles did not significantly alter the viability of the fibroblasts in a broad range of concentrations (from 25 to 500 μg $mL^{-1}$; Fig. 7). Only concentrations higher than 700 μg $mL^{-1}$ significantly reduced cell viability (29.76% compared to untreated control levels). Thus, we can conclude that MAC–PEI microporous particles at concentrations intended for biomedical applications exert negligible cytotoxic effects.

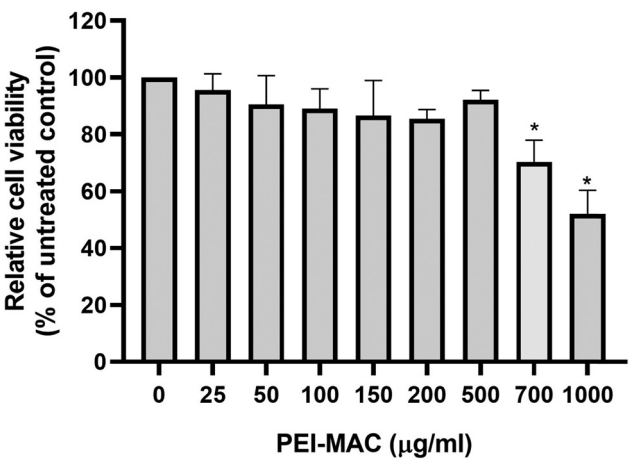


Fig. 7 Effects of MAC–PEI on M1 human skin fibroblasts viability. Cell was tested after 24 h exposure to MAC–PEI (0–1000 μg $ml^{-1}$). Data are shown as the mean ± SEM of 3 independent experiments and expressed as a percentage of untreated control levels. Cytotoxicity assays were performed in triplicates per experimental condition. Statistical significance was established at $p$ values below or equal to 0.05 (*).

### 3.5. Methotrexate vehiculation and controlled drug release. Effect of external stimuli

As mentioned above, a calibration was first performed to determine the concentration of adsorbed and released MTX (data in Fig. S3, ESI†). In addition, adsorption kinetics tests (solutions 0.6 mM MTX, particle concentration 6 mg $mL^{-1}$) were performed in the range of 1, 2, 24, 72, 144 h, showing that adsorption in the first two hours exceeded 80% (Fig. S4, ESI†). For the sake of comparison, experiments were also performed on MAC particles without PEI coating, and it was found that 76% MTX was adsorbed in the same conditions. This suggests that the high porosity of the MAC particles is largely responsible for the total adsorption found. Further evidence of this high MTX loading is provided by drug adsorption tests (up to 10 mM) in which the MAC–PEI sample adsorbed almost all the drug brought into contact with the particles (Fig. S5, ESI†).

As can be seen in Fig. 8, drug release at pH 5.8, which mimics the tumor environment, is significantly enhanced by the application of external stimuli such as photothermia and rotating fields. Drug release induced by laser irradiation on magnetic particles has been described by other authors with different drugs such as AS-48[69] or doxorubicin.[70] In the latter study, mesoporous silica particles with a magnetic core loaded between 20% and 40% of the drug, which allows us to conclude that: (1) MAC particles are a more effective alternative for drug loading than conventional magnetic particles and even mesoporous silica with a magnetic core, since they load almost all the drug available in the solution due to their high specific surface area, and (2) although the release may seem low (around 4%), the large amount of drug adsorbed in absolute terms is sufficient to optimise future anti-tumour treatments compared to other studies such as the one mentioned above or to our previous work with doxorubicin and PEI-coated magnetite particles (5 μmol $g^{-1}$ drug release in the best conditions[33]).

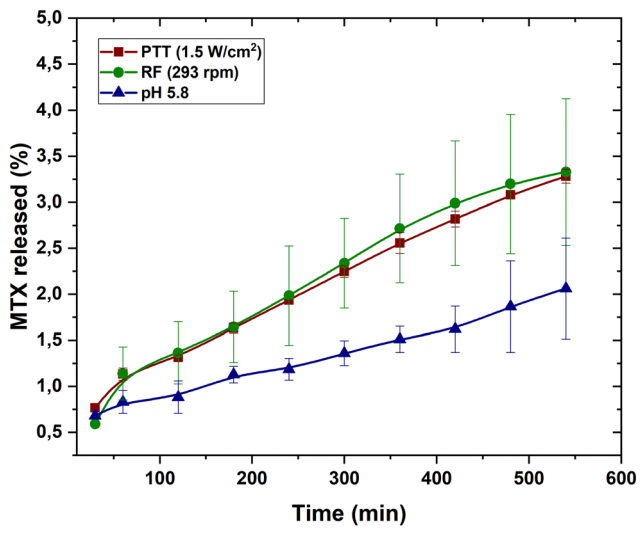


Fig. 8 Release of MTX with respect to the amount previously adsorbed on PEI-coated MAC particles using different stimuli: photothermal therapy (PTT), rotating fields (RF), and with no stimuli applied, all of them in phosphate buffer at pH 5.8.

Fig. 8 also shows that drug release using rotating fields slightly improves release performance, probably due to mechanically enhanced diffusion. In general, the release achieved under either PTT or MRF is significantly higher compared to our results under non stimulated conditions. The latter were also investigated at pH 7.4, as depicted in Fig. S6 (ESI†): although at this pH the drug tends to be released more rapidly initially, this is not of great significance, as the time that the particles typically would employ to reach the target organ would be much shorter (blood completes a full circulation through the vascular system within minutes), and so no significant release would have occurred during the transit. In fact, the drug administration times are much longer, and hence the period of interest for observation would be in the range of hours. In this case, the drug release under stimuli (with particles already at the acidic tumor pH) is larger than without rotating magnetic field or photothermia (Fig. 8). Similar results have been reported by Nappini *et al.*,[71] who observed that magnetoliposomes loaded with carboxyfluorescein experienced a significantly enhanced release of the fluorescent agent under the influence of a low-frequency alternating magnetic field (5.8 kHz). This is a very interesting result, as this technique has been less studied and could be more effective than photothermia for biomedical applications requiring high tissue penetration.

## 4. Conclusions

This work describes the utilisation of porous activated carbon particles as vehicles for the anti-tumour drug MTX. The particles are coated with magnetite nanoparticles, which confer them superparamagnetic behaviour, thus extending the field of application to situations where it is possible to use external magnetic fields to transport the particles to their action site or eventually produce heating if the field is alternating, or torque if the magnetic field is rotating. To enhance the stability of the particles and their interaction with the anti-tumour agent, a cationic polymer, low molecular weight PEI, is employed for their coating. The MAC–PEI particles demonstrate high biocompatibility at concentrations suitable for biomedical applications, and exhibit a photothermal response to infrared laser irradiation, whereby local heating is generated. This phenomenon is exploited in this research as a stimulus to enhance MTX release. The photothermal response is markedly elevated for the activated carbon-magnetite (MAC) composites, and it is little affected by the application of the polymer coating. The synthesised MAC–PEI composite particles demonstrated the capacity to adsorb up to 80% of the drug from a 0.6 mM MTX solution after 20 hours of contact. The drug release was conducted at pH 5.8 with and without the application of external photothermal and rotating magnetic field stimuli. The process is gradual and can be controlled using stimuli of different intensity, resulting in a considerable increase in the amount of drug released. The designed porous particles thus appear to be excellent smart platforms for the transport and release of MTX, as they can load significant quantities of drug and releasing it

gradually at a rate that can be controlled by both PTT and RMF external stimuli, while preserving biocompatibility.

## Data availability

The data used to support the finding of this study are included within the article and ESI.†

## Conflicts of interest

The authors declare that they have no competing interests. The funders had no role in the design of the study; in the collection, analysis, or interpretation of data; in the writing of the manuscript, or in the decision to publish the results.

## Acknowledgements

Financial support of this investigation by the grant TED2021-131855BI00/AEI/10.13039/501100011033/Unión Europea Next Generation EU/PRTR and PID2023-151881OB-I00 MICIU/AEI/10.13039/501100011033/and FEDER, EU is gratefully acknowledged. We also thank Juan M. Falcón-Perez (Metabolomics Unit, Centro de Investigación Cooperativa en Biociencias, Derio, Vizcaya, Spain) for providing M1 human fibroblasts, and Pedro Urquiza (Torrecárdenas University Hospital, Biomedical Research Unit-Biotechnology Laboratory, Almería, Spain) for his technical assistance with them. TR is the recipient of a Ramón y Cajal RYC2022-035807.

## References

1 E. Laconi, F. Marongiu and J. DeGregori, *Br. J. Cancer*, 2020, **122**, 943–952.
2 S. Pilleron, E. Soto-Perez-de-Celis, J. Vignat, J. Ferlay, I. Soerjomataram, F. Bray and D. Sarfati, *Int. J. Cancer*, 2021, **148**, 601–608.
3 F. Fernández-Alvarez, C. Caro, G. García-García, M. L. García-Martín and J. L. Arias, *J. Mater. Chem. B*, 2021, **9**, 4963–4980.
4 F. Fernandez-Alvarez, G. García-García and J. L. Arias, *Pharmaceutics*, 2021, **13**, 1232.
5 P. T. Ribeiro, J. A. Moreira, J. F. Monterio and S. M. Laranjeira, *J. Controlled Release*, 2022, **347**, 89–103.
6 K. Loomis, K. McNeeley and R. V. Bellamkonda, *Soft Matter*, 2011, **7**, 839–856.
7 K. Y. Choi, G. Liu, S. Lee and X. Chen, *Nanoscale*, 2012, **4**, 330–342.
8 M. E. Davis, *MRS Bull.*, 2012, **37**, 828–835.
9 R. Wang, P. S. Billone and W. M. Mullett, *J. Nanomater.*, 2013, **2013**, 629681.
10 L. N. Toksvang, S. H. R. Lee, J. J. Yang and K. Schmiegelow, *Leukemia*, 2022, **36**, 1749–1758.
11 B. Zhang, Y. Zhang, R. Z. Li, J. Z. Li and X. C. Lu, *J. Orthop. Surg. Res.*, 2020, **15**, 5101–5128.
12 J. May, K. R. Carson, S. Butler, W. J. Liu, N. L. Bartlett and N. D. Wagner-Johnston, *Leuk. Lymphoma*, 2014, **55**, 1345–1349.
13 H. Shariatifar, F. Ranjbarian, F. Hajiahmadi and A. Farasat, *Mol. Biol. Rep.*, 2022, **49**, 11049–11060.
14 L. B. Ramsey, F. M. Balis, M. M. O'Brien, K. Schmiegelow, J. L. Pauley, A. Bleyer, B. C. Widemann, D. Askenazi, S. Bergeron, A. Shirali, S. Schwartz, A. A. Vinks and J. Heldrup, *Oncologist*, 2018, **23**, 52–61.
15 Y. Y. Yang, C. Y. Wang, Y. T. Chen, X. B. Wang, Z. Jiao and Z. Wang, *Eur. J. Pharm. Sci.*, 2023, **186**, 106416.
16 D. Banerjee, P. Mayer-Kuckuk, G. Capiaux, T. Budak-Alpdogan, R. Gorlick and J. R. Bertino, *Biochim. Biophys. Acta, Mol. Basis Dis.*, 2002, **1587**, 164–173.
17 Z. A. Khan, R. Tripathi and B. Mishra, *Expert Opin. Drug Delivery*, 2012, **9**, 151–169.
18 G. Choi, T. H. Kim, J. M. Oh and J. H. Choy, *Coord. Chem. Rev.*, 2018, **359**, 32–51.
19 M. Thangavelu, A. Adithan, S. T. Parvathaleswara and C. Munusamy, *Pharm. Res.*, 2018, **35**, 184.
20 T. H. Hsin, N. Dhenadhayalan and K. C. Lin, *ACS Appl. Biomater.*, 2020, **3**, 8786–8794.
21 F. Guo, X. Mao, J. Wang, F. Luo and Z. Wang, *J. Int. Med. Res.*, 2011, **39**, 2217–2227.
22 N. Miriyala, D. F. Ouyang, Y. Perrie, D. Lowry and D. J. Kirby, *Eur. J. Pharm. Biopharm.*, 2017, **115**, 197–205.
23 K. R. Olson, *J. Med. Toxicol.*, 2010, **6**, 190–198.
24 S. K. Shahcheragh, M. M. B. Mohagheghi and A. Shirpay, *SN Appl. Sci.*, 2023, **5**(12), 313.
25 X. Y. Li, Y. Shimizu, A. Pyatenko, H. Q. Wang and N. Koshizaki, *J. Mater. Chem.*, 2011, **21**, 14406–14409.
26 A. Espinosa, J. Kolosnjaj-Tabi, A. Abou-Hassan, A. P. Sangnier, A. Curcio, A. K. A. Silva, R. Di Corato, S. Neveu, T. Pellegrino, L. M. Liz-Marzan and C. Wilhelm, *Adv. Funct. Mater.*, 2018, **28**(37), 1803660.
27 H. Belkahla, R. Boudjemaa, V. Caorsi, D. Pineau, A. Curcio, J. S. Lomas, P. Decors, A. Chevillot-Biraud, T. Azais, C. Wilhelm, H. Randriamahazaka and M. Hemadi, *Nanoscale Adv.*, 2019, **1**, 2571–2579.
28 X. S. Li, J. F. Lovell, J. Yoon and X. Y. Chen, *Nat. Rev. Clin. Oncol.*, 2020, **17**, 657–674.
29 L. H. Reddy, J. L. Arias, J. Nicolas and P. Couvreur, *Chem. Rev.*, 2012, **112**, 5818–5878.
30 T. J. Yu, P. H. Li, T. W. Tseng and Y. C. Chen, *Nanomedicine*, 2011, **6**, 1353–1363.
31 M. Y. Liao, P. S. Lai, H. P. Yu, H. P. Lin and C. C. Huang, *Chem. Commun.*, 2012, **48**, 5319–5321.
32 M. Q. Chu, Y. X. Shao, J. L. Peng, X. Y. Dai, H. K. Li, Q. S. Wu and D. L. Shi, *Biomaterials*, 2013, **34**, 4078–4088.
33 M. Lazaro, P. Lupianez, J. L. Arias, M. P. Carrasco-Jimenez, A. V. Delgado and G. R. Iglesias, *Polymers*, 2022, **14**, 4913.
34 X. Hua, Q. Yang, Z. Dong, J. Zhang, W. Zhang, Q. Wang, S. Tan and H. Smyth, *Drug Delivery*, 2017, **24**, 511–518.
35 T. Marín, P. Montoya, O. Arnache, R. Pinal and J. Calderón, *Mater. Des.*, 2018, **152**, 78–87.
36 S. Cho, N. Min, W. Park, S. Kim and D. Kim, *Adv. Funct. Mater.*, 2019, **29**, 1901384.

37 Y. Cheng, M. Muroski, D. Petit, R. Mansell, T. Vemulkar, R. Morshed, Y. Han, I. Balyasnikova, C. Horbinski, X. Huang, L. Zhang, R. Cowburn and M. Lesniak, *J. Controlled Release*, 2016, **223**, 75–84.
38 J. Zhao, C. Lu, X. He, X. Zhang, W. Zhang and X. Zhang, *ACS Appl. Mater. Interfaces*, 2015, **7**, 2607–2615.
39 X. Sun, C. Cai, Q. Wang, D. Cai, J. Qian, Y. Chi, K. Zheng, X. Zhang, G. Zhang, K. Zhong and Z. Wu, *Phys. Chem. Chem. Phys.*, 2016, **18**, 7820–7828.
40 M. Lázaro, A. Sola-Leyva, M. Jimenez-Carretero, M. Jiménez, A. Delgado and G. Iglesias, *J. Drug Delivery Sci. Technol.*, 2024, **95**, 105622.
41 M. D. Ramos-Tejada, J. L. Viota, K. Rudzka and A. V. Delgado, *Colloids Surf., B*, 2015, **128**, 1–7.
42 B. Chertok, A. David and V. Yang, *Biomaterials*, 2010, **31**, 6317–6324.
43 E. dos-Santos-Silva, M. Alves-Silva, J. de Medeiros, R. dos Santos-Cavalcante, A. Cornélio, M. Fernandes-Pedrosa, E. do Egito, R. de Araujo and A. da Silva, *J. Mol. Liq.*, 2020, **315**, 113721.
44 R. Goyal, S. K. Tripathi, E. Vazquez, P. Kumar and K. C. Gupta, *Biomacromolecules*, 2012, **13**, 73–83.
45 M. Ramos-Tejada, J. Viota, K. Rudzka and A. Delgado, *Colloids Surf., B*, 2015, **128**, 1–7.
46 A. Alexander, A. Pillai, V. Manikantan, G. Varalakshmi, B. Akash and I. Enoch, *Mater. Lett.*, 2022, **313**, 131830.
47 A. Balan, M. M. R. Kennedy, V. Manikantan, A. Alexander, G. S. Varalakshmi, S. Ramasamy, A. S. Pillai and I. V. M. V. Enoch, *Bull. Mater. Sci.*, 2024, **47**, 28.
48 M. Williams, S. Grace, V. Manikantan, A. Alexander, G. Varalakshmi, S. Ramasamy, A. Pillai, I. Enoch and D. Núñez, *Mater. Lett.*, 2024, **355**, 135540.
49 Z. Nazarkina, T. Savostyanova, B. Chelobanov, I. Romanova, P. Simonov, R. Kvon, A. Karpenko and P. Laktionov, *Pharmaceutics*, 2022, **14**, 6713.
50 B. Sanz, M. P. Calatayud, N. Cassinelli, M. R. Ibarra and G. F. Goya, *Eur. J. Inorg. Chem.*, 2015, 4524–4531.
51 P. Urquiza, A. Laín, A. Sanz-Parra, J. Moreno, G. Bernardo-Seisdedos, P. Dubus, E. González, V. Gutiérrez-de-Juan, S. García, H. Eraña, I. Juan, I. Macías, F. Ben Bdira, P. Pluta, G. Ortega, J. Oyarzábal, R. González-Muñiz, J. Rodríguez-Cuesta, J. Anguita, E. Díez, J. Blouin, H. de Verneuil, J. Mato, E. Richard, J. Falcón-Pérez, J. Castilla and O. Millet, *Sci. Transl. Med.*, 2018, **10**, eaat7467.
52 S. Bhattacharjee, *J. Controlled Release*, 2016, **235**, 337–351.
53 G. García-García, M. Lázaro-Callejón, F. Fernández-Alvarez, G. R. Iglesias and J. L. Arias, *J. Magn. Magn. Mater.*, 2023, **588**, 171500.
54 F. Ahmadijokani, S. Tajahmadi, M. Rezakazemi, A. Sehat, H. Molavi, T. Aminabhavi and M. Arjmand, *J. Environ. Manage.*, 2021, **277**, 111448.
55 H. Javadian, F. Ghorbani, H. Tayebi and S. Asl, *Arabian J. Chem.*, 2015, **8**, 837–849.
56 G. García-García, F. Fernández-Alvarez, L. Cabeza, A. Delgado, C. Melguizo, J. Prados and J. Arias, *Polymers*, 2020, **12**, 2790.
57 T. Maneerung, J. Liew, Y. Dai, S. Kawi, C. Chong and C. Wang, *Bioresour. Technol.*, 2016, **200**, 350–359.
58 S. Sambaza, M. Masheane, S. Malinga, E. Nxumalo and S. Mhlanga, *Phys. Chem. Earth*, 2017, **100**, 236–246.
59 S. Kemp, R. Ferguson, A. Khandhar and K. Krishnan, *RSC Adv.*, 2016, **6**, 77452–77464.
60 N. Bayliss and B. Schmidt, *Prog. Polym. Sci.*, 2023, **147**, 101753.
61 J. Akoto, F. Chai, E. Repo, Z. Yang, D. Wang, F. Zhao, Q. Liao and L. Chai, *J. Environ. Chem. Eng.*, 2022, **10**, 108589.
62 R. Megias, M. Arco, J. Ciriza, L. del Burgo, G. Puras, M. López-Viota, A. Delgado, J. Dobson, J. Arias and J. Pedraz, *Int. J. Pharm.*, 2017, **518**, 270–280.
63 A. Bucharskaya, G. Maslyakova, G. Terentyuk, A. Yakunin, Y. Avetisyan, O. Bibikova, E. Tuchina, B. Khlebtsov, N. Khlebtsov and V. Tuchin, *Int. J. Mol. Sci.*, 2016, **17**, 1295.
64 S. Jacques, *Surg. Clin. North Am.*, 1992, **72**, 531–558.
65 A. Gobin, M. Lee, N. Halas, W. James, R. Drezek and J. West, *Nano Lett.*, 2007, **7**, 1929–1934.
66 S. Cabana, A. Curcio, A. Michel, C. Wilhelm and A. Abou-Hassan, *Nanomaterials*, 2020, **10**, 1548.
67 A. Wlodarczyk, S. Gorgon, A. Radon and K. Bajdak-Rusinek, *Nanomaterials*, 2022, **12**, 1807.
68 M. Chu, J. Peng, J. Zhao, S. Liang, Y. Shao and Q. Wu, *Biomaterials*, 2013, **34**, 1820–1832.
69 S. C. Gaglio, Y. Jabalera, M. Montalban-Lopez, A. C. Millan-Placer, M. Lazaro-Callejon, M. Maqueda, M. P. Carrasco-Jimenez, A. Laso, J. A. Ainsa, G. R. Iglesias, M. Perduca and C. J. Lopez, *Pharmaceutics*, 2022, **14**, 2744.
70 A. Adam, S. Harlepp, F. Ghilini, G. Cotin, B. Freis, J. Goetz, S. Bégin, M. Tasso and D. Mertz, *Colloids Surf., A*, 2022, **640**, 128407.
71 S. Nappini, F. Bombelli, M. Bonini, B. Nordèn and P. Baglioni, *Soft Matter*, 2010, **6**, 154–162.